Multiscale topology optimization of an electromechanical dynamic energy harvester made of non-piezoelectric material

Xing Chen, Song Yao, Julien Yvonnet

Multiscale topology optimization of an electromechanical dynamic energy harvester made of non-piezoelectric material

Xing Chen,[1, 2] Song Yao,[1] and Julien Yvonnet[2, a)]

[1)]*Key Laboratory of Traffic Safety on Track, Ministry of Education, School of Traffic & Transportation Engineering, Central South University, Changsha 410075, China*

[2)]*Université Gustave Eiffel, CNRS, MSME UMR 8208, F-77454 Marne-la-Vallée, France*

(Dated: 13 November 2024)

Abstract In this work, a novel multiscale topology optimization method has been proposed for the design of electromechanical energy harvesting systems converting mechanical vibrations into electric currents made of non-piezoelectric materials. At the microscopic scale, the material is assumed to be periodic, porous and flexoelectric, although not piezoelectric. A first step of topology optimization is performed, in order to maximize the effective (homogenized) flexoelectric properties of the material, where a flexoelectric homogenization model is first formulated. As a result, the effective material, although made of a non-piezoelectric material, has apparent piezoelectric properties. In a second step, these properties are used to model the behaviour of a dynamic electromechanical energy harvesting system structure. A second topology optimization step, this time performed at the structural scale, aims to maximize the system Electromechanical Coupling Factor (ECF) for a given forced vibration frequency, including the micro-inertial effect. At both scales, an Isogeometric Analysis (IGA) method is employed to solve the strain-gradient problems numerically. We show that the optimized structure obtained offers significant gains in terms of ECF (by a factor of between 2 and 20) compared with non-optimized structures of the same volume, over a wide range of excitation frequencies. The procedure could open up new possibilities in the design of energy recovery systems without the use of piezoelectric materials.

[a)]Electronic mail: julien.yvonnet@u-pem.fr

I. INTRODUCTION

In recent decades, there has been considerable interest in converting ambient vibrational energy into electrical energy to power micro and nanoelectronics. Piezoelectric materials, which act as transducers between mechanical and electrical stimuli, have found applications in a variety of energy-harvesting devices[?] . As electronic devices continue to shrink in size, the use of micro- and nanoscale piezoelectric energy sensors is receiving increasing attention. However, piezoelectricity is limited to non-centrosymmetric crystalline materials, and piezoelectric devices are often prone to electrical fatigue, particularly when exposed to high-frequency vibrations. Recently, the flexoelectric effect has received increasing attention, both theoretically and practically. Flexoelectricity exists in all dielectric materials and increases with decreasing sample size. Thanks to these properties, it ideally offers low-cost alternatives to conventional piezoelectric materials for electromechanical devices.

Flexoelectricity, which refers to the linear relationship between electrical polarization and strain gradient, was first predicted by Mashkevich and Tolpygo[?] in the 1950s, and then observed experimentally by Harris[?] . Kogan[?] estimated the range of flexoelectric coefficients for several materials. Numerous studies have focused on solving the fourth-order partial differential equations of flexoelectricity in solids using analytical models[? ? ? ?] on simplified geometries, and numerical methods[? ? ? ? ? ? ? ? ? ?] on more complex geometries. Reviews and discussions exploring theoretical and experimental research, as well as computational frameworks, can be found in the literature[? ? ? ?] .

The challenges for flexoelectrics are to improve electromechanical coupling effects, and to use a wider range of materials than hard ceramics. Flexoelectric structures, made from a single material but shaped to induce significant gradients, open up new possibilities. These structures, fabricated from suitable flexoelectric materials, feature versatile functionalities such as sensing, actuation and power generation. In the realm of flexoelectric composites, research has concentrated on developing piezoelectric composites using non-piezoelectric materials, driven by earlier work[? ?] . Traditional piezoelectric composites usually include lead-containing PZT for higher permittivity[?] . Ppiezoelectric responses can be achieved in these composites made of purely flexoelectric materials, which are comparable to common single-phase piezoelectrics. These two lines of research motivate our further exploration and design of flexoelectric structures and flexoelectric composites for enhanced and sustainable electromechanical applications. Several approaches

have been proposed to increase flexoelectric constants in solids, such as the use of electrets[?] and architecture materials[?] .

More recently, topological optimization (TO) has emerged as a promising method for improving apparent flexoelectricity and electromechanical coupling factors in piezoelectric and flexoelectric structures. The primary objective of topological optimization is to determine the distribution of materials in a specified domain without pre-existing knowledge in order to obtain the best structural performance[? ? ? ? ?] . The TO optimization process relies on information about the gradient of the objective function with respect to the design variables. In contrast to gradient-free optimization approaches (such as genetic algorithms, particle swarms, cuckoo search and Jaya et al.[? ? ? ? ? ?]), which do not require gradient information and can produce discrete 0-1 designs, the gradient-based continuous optimization algorithm exhibits superior resolution efficiency, particularly in finer-mesh scenarios. In recent years, the focus has been on integrating machine learning/deep learning with structural optimization[? ?] .

Several works have been dedicated to the optimization of composites and energy harvesters with flexoelectricity and piezoelectricity. Chen[? ?] et al. have developed a topology optimization framework aimed at designing periodic composites comprising piezoelectric constituents, resulting in an increase in direct and converse flexoelectric constants, where a Representative Volume Element (RVE)-based computational homogenization was employed to estimate the effective flexoelectric properties. Ghasemi[?] et al. proposed an optimization design methodology for piezoelectric/flexoelectric materials, employing a Iso Geometric Analysis (IGA) and the Level-set topology optimization approach, and successfully applied it to the multi-material design of flexoelectric composites. Nanthakumar[?] et al. have developed a level-set based topology optimization to maximize the electromechanical coupling factor of flexoelectric nanostructures, by solving the flexoelectric PDEs through a mixed finite element formulation. Jorge[?] et al. developed a shape and topology optimization method based on an isogeometric phase field to improve the effective electromechanical coupling factor of flexoelectric structures. Zhang[?] et al proposed an explicit topology optimization to improve the electromechanical coupling factors and effective electric polarization of flexoelectric nanostructures, using the Moving Morphable Void and IGA-based approach. Some works have been devoted to the topology optimization of piezoelectric energy harvesters accounting for static and harmonic dynamic mechanical loads[? ? ?] . Silva et al. employed topology optimization in combination with homogenization method to design piezocomposite materials[?] and then piezoelectric transducers[?] . The universality and outstanding scaling ef-

fect of the flexoelectric effect are promising for designing advanced nano/micro-electromechanical systems (N/MEMS).

Although remarkable progress has been made in improving flexoelectric properties through topological optimization methods, there is little work on optimizing dynamic flexoelectric structures. To fully exploit the potential of flexoelectric properties in practical applications, it is essential to optimize flexoelectric microstructures to improve their effective behavior. By integrating the design of the microstructure with the optimization of the energy sensor structure, a much more significant improvement in the efficiency of the electromechanical coupling is potentially possible.

In this work, a multi-scale topological optimization framework for micro and macro flexoelectric structures is proposed, with the aim of improving the effective flexoelectric properties and dynamic electromechanical coupling efficiency of energy harvesting systems. The micro and macro dynamic electromechanical equations are solved using iso-geometric analysis (IGA). Isogeometric analysis is widely applied to structural analysis because of its advantage in constructing high-order continuity[? ? ? ? ?], and is employed to ensure C^1 continuity of the approximate displacement deposited. To numerically evaluate the effective flexoelectric behavior of microstructures, we introduce a flexoelectric homogenization model, which is then combined with structure-scale topology optimization to design both structure and microstructure geometry to optimize flexoelectric properties.

Specifically, we tailor the microstructures to maximize the flexoelectric component that characterizes polarization under bending deformation. We then use the optimized flexoelectric microstructures to derive a homogenized flexoelectric model, which is used in the topology-optimized structural model. To guarantee structural integrity and connectivity, we impose a compliance constraint in the optimization process of the dynamic energy harvester.

II. HOMOGENIZATION OF HETEROGENEOUS FLEXOELECTRIC MATERIALS

We first present a framework to perform the homogenization of microstructures made of flexoelectric materials. We consider a periodic composite (see Fig. **??** (a)) characterized by a Representative Volume Element (RVE) defined in a domain $\Omega_m \in \mathbb{R}^2$ whose boundary is denoted by $\partial\Omega_m$, as shown schematically in Fig.**??** (b). The phases within the RVE are assumed to be linearly flexoelectric and characterized by an elastic tensor C, a dielectric tensor α and a flexoeletric tensor μ. The energy density function of a purely flexoelectric material (non-piezoelectric) at the

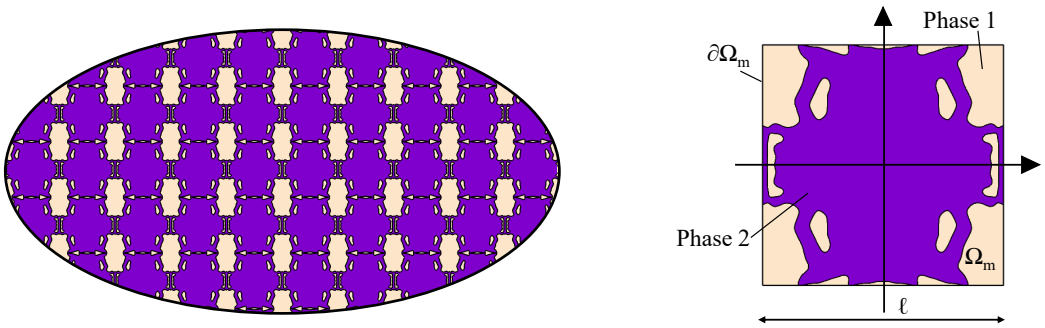

(a) (b)

FIG. 1: (a) Periodic flexoelectric structure and (b) Representative Volume Element (RVE) made of two phases.

microscale is defined by:

$$W_1 = \frac{1}{2}C_{ijkl}\varepsilon_{ij}\varepsilon_{kl} - \frac{1}{2}\alpha_{ij}E_iE_j - \mu_{ijkl}E_i\nabla\varepsilon_{jkl} \tag{1}$$

where ε denotes strain tensor, E denotes electric field vector, related to the electric potential ϕ by $E_i = -\phi_{,i}$, and $\nabla\varepsilon$ dnotes the third-order strain gradient tensor.

The local equilibrium equations are given by

$$\sigma_{ij,j} - \tau_{ijk,jk} - f_i = R_{1i} = 0, \text{ in } \Omega_m \tag{2}$$

$$d_{i,i} = R_2 = 0, \text{ in } \Omega_m \tag{3}$$

with:

$$\sigma_{ij} = C_{ijkl}\varepsilon_{kl} \tag{4}$$

$$d_i = \alpha_{ij}E_j + \mu_{ijkl}\nabla\varepsilon_{jkl} \tag{5}$$

$$\tau_{jkl} = -\mu_{ijkl}E_i \tag{6}$$

where σ denotes the stress tensor, f denotes body forces vector, d denotes the electric displacement, and τ denotes the couple stress. The RVE is assumed to be subjected to macroscopic loads, i.e. a macroscopic strain $\overline{\varepsilon}$, a macroscopic electric field $\overline{E}$ and a macroscopic strain gradient $\overline{\nabla\varepsilon}$ which are defined at the scale of the structure. They are transferred to the RVE through the quadratic boundary conditions:

$$u_i = \overline{\varepsilon}_{ij} x_j + \frac{1}{2}\overline{g}_{ijk} x_j x_k + \tilde{u}_i \text{ on } \partial\Omega_m \tag{7}$$

with

$$\overline{g}_{ijk} = \overline{\nabla\varepsilon}_{ijk} + \overline{\nabla\varepsilon}_{ikj} - \overline{\nabla\varepsilon}_{jki} \tag{8}$$

and

$$\phi = -\overline{E}_i x_i \text{ on } \partial\Omega_m \tag{9}$$

The forces f in (**??**) have been introduced in[**?**] to induce purely uniform fields of derivatives when the RVE is homogeneous. Their expression is given by:

$$f_i = \overline{C}_{ijkl}\overline{\nabla\varepsilon}_{klj} \tag{10}$$

$$\tag{11}$$

Using superposition, the local strain field $\varepsilon(x)$, local electric field $E(x)$ and local strain gradient field $\nabla\varepsilon(x)$ at a point $x \in \Omega_m$ can be expressed in the form[**?**] :

$$\varepsilon_{ij}(x) = A^0_{ijpq}(x)\overline{\varepsilon}_{pq} - B^0_{ijp}(x)\overline{E}_p - A^1_{ijpqr}(x)\overline{\nabla\varepsilon}_{pqr} \tag{12}$$

$$E_i(x) = D^0_{ipq}(x)\overline{\varepsilon}_{pq} - h^0_{ip}(x)\overline{E}_p - D^1_{ipqr}(x)\overline{\nabla\varepsilon}_{pqr} \tag{13}$$

$$\nabla\varepsilon_{ijk}(x) = J^0_{ijkpq}(x)\overline{\varepsilon}_{pq} - Q^0_{ijkp}(x)\overline{E}_p - J^1_{ijkpqr}(x)\overline{\nabla\varepsilon}_{pqr} \tag{14}$$

where the local fields A^0, B^0, A^1, D^0, A^0, h^0, D^1, J^0, Q^0 and J^1 are obtained by solving Eqs. (**??**) and (**??**) on the RVE by the Isogeometric Analysis method (IGA). More details are provided in Appendix.**??**). Substituting (**??**)-(**??**) into (**??**), the effective (homogenized) flexoelectric tensor is obtained as:

$$\overline{\mu}_{ijkl} = \left\langle -B^0_{pqi}C_{pqrs}A^1_{rsjkl} + h^0_{pi}\alpha_{pq}D^1_{qjkl} + Q^0_{pqri}\mu_{pqrs}D^1_{sjkl} + h^0_{pi}\mu_{pqrs}J^1_{qrsjkl} \right\rangle \tag{15}$$

where $\langle\cdot\rangle = \frac{1}{V}\int(\cdot)dV$. In the above, the dependence to x has been ommitted to alleviate the notations. The 2D matrix form of the effective flexoelectric tensor can be written as:

$$\overline{\boldsymbol{\mu}} = \begin{bmatrix} \overline{\mu}_{1111} & \overline{\mu}_{1112} & \overline{\mu}_{1221} & \overline{\mu}_{1222} & \overline{\mu}_{1121} & \overline{\mu}_{1122} \\ \overline{\mu}_{2111} & \overline{\mu}_{2112} & \overline{\mu}_{2221} & \overline{\mu}_{2222} & \overline{\mu}_{2121} & \overline{\mu}_{2122} \end{bmatrix} \tag{16}$$

III. DYNAMIC FLEXOELECTRICITY AT THE MACRO SCALE

We consider a structure defined in an open domain $\Omega \subset \mathbb{R}^2$, with boundary $\partial\Omega$, and associated with the macro scale problem. At this scale, the composite is modeled by a homogeneous material whose effective properties have been defined with respect to a given microstructure geometry in section **??**. Over the boundary of the domain $\partial\Omega$, mechanical displacements and tractions are prescribed over parts of the boundary denoted respectively by $\partial\Omega_u$ and $\partial\Omega_t$, as well as electric potential and surface charge density over portions $\partial\Omega_\phi$ and $\partial\Omega_D$, respectively. In addition, the strain gradients are associated with other types of boundary conditions defined over portions of the boundary $\partial\Omega_v$ and $\partial\Omega_r$. The boundary conditions are imposed such that $\partial\Omega_u \cup \partial\Omega_t = \partial\Omega_\phi \cup \partial\Omega_D = \partial\Omega_v \cup \partial\Omega_r = \partial\Omega$ and $\partial\Omega_u \cap \partial\Omega_t = \partial\Omega_\phi \cap \partial\Omega_D = \partial\Omega_v \cap \partial\Omega_r = \emptyset$. We define the electric enthalpy density $\hat{h}$ for a linear electromechanical system as (more details in**?**):

$$\hat{h} = \frac{1}{2}\overline{C}_{ijkl}\varepsilon_{ij}\varepsilon_{kl} - \frac{1}{2}\overline{\alpha}_{ij}E_iE_j - \overline{e}_{ijk}E_k\varepsilon_{ij} - \overline{\mu}_{ijkl}E_i\nabla\varepsilon_{jkl} + \frac{1}{2}\overline{G}_{ijklmn}\nabla\varepsilon_{ijk}\nabla\varepsilon_{lmn} \tag{17}$$

where $\overline{C}$, $\overline{\alpha}$, $\overline{e}$ and $\overline{\mu}$ are the effective (homogenized) elastic, dielectric, piezoelectric and flexoelectric tensors, respectively, while $\overline{G}$ corresponds to the higher-order strain gradient elastic tensor (see a complete definition of these tensors in**?**). For the sake of simplification, we assume here $\overline{G}$ in the form: $\overline{G}_{ijklmn} = \overline{C}_{ijlm}\ell_{kn}$, where ℓ_{kn} are material length parameters. Note that in this section, we do not use special notation to differ the quantities from microscopic ones in the previous section, to avoid burdening the notations.

The electric field vector E_j, the strain tensor ε_{ij} and strain-gradient tensor $\nabla\varepsilon_{ijk}$ are defined as:

$$E_j = -\phi_{,j} \tag{18}$$

$$\varepsilon_{ij} = \frac{1}{2}(u_{i,j} + u_{j,i}) \tag{19}$$

$$\nabla\varepsilon_{ijk} = \varepsilon_{ij,k} = \frac{1}{2}(u_{i,jk} + u_{j,ik}) \tag{20}$$

The constitutive equations are derived as:

$$d_i = -\frac{\partial\hat{h}}{\partial E_i} = \overline{\alpha}_{ij}E_j + \overline{e}_{ijk}\varepsilon_{jk} + \overline{\mu}_{ijkl}\nabla\varepsilon_{jkl} \tag{21}$$

$$\sigma_{ij} = \frac{\partial\hat{h}}{\partial\varepsilon_{ij}} = \overline{C}_{ijkl}\varepsilon_{kl} - \overline{e}_{ijk}E_k \tag{22}$$

$$\tau_{ijk} = \frac{\partial\hat{h}}{\partial\nabla\varepsilon_{ijk}} = \overline{G}_{ijklmn}\nabla\varepsilon_{lmn} - \overline{\mu}_{ijkl}E_l \tag{23}$$

By integrating over Ω we obtain the electrical enthalpy as

$$H = \frac{1}{2}\int_{\Omega}(\sigma_{ij}\varepsilon_{ij} + \tau_{ijk}\nabla\varepsilon_{ijk} - D_i E_i)d\Omega \tag{24}$$

The work W of external mechanical and electrical forces are given as

$$W^{ext} = \int_{\Omega_t} t_i^d u_i dS - \int_{\Omega_D} D_n^b \phi dS \tag{25}$$

The Rayleigh dissipation can be written as

$$\tilde{R} = \frac{1}{2}\int_{\Omega} V_{ij}\dot{u}_i\dot{u}_j d\Omega \tag{26}$$

where V_{ij} is viscous damping coefficients and $\dot{(\cdot)}$ is time derivative.

The kinetic energy taking into account micro-inertial effect is defined by

$$K = \frac{1}{2}\int_{\Omega}\rho_0(\dot{u}_i\dot{u}_i + \ell_d^2\dot{u}_{i,j}\dot{u}_{i,j})d\Omega \tag{27}$$

where ρ_0 is the density, ℓ_d is a dynamic scaling parameter (micro inertia characteristic length). The acceleration gradient term is generally introduced to obtain physically acceptable dispersive wave velocity[?] in strain-gradient models.

The governing differential equations for the electromechanical system are derived from the Hamilton's principle:

$$\delta\int_{t_1}^{t_2}(H - W - K)dt = 0 \tag{28}$$

After algebraic manipulation, the weak form of balance equations are obtained as:

$$\int_{\Omega}\left(\rho_0\ddot{u}_i\delta u_i + \ell_d^2\ddot{u}_{i,j}\delta u_{i,j} + \sigma_{ij}\delta\varepsilon_{ij} + \tau_{ijk}\delta\nabla\varepsilon_{ijk} + V_{ij}\dot{u}_i\delta u_j\right)d\Omega - \int_{\partial\Omega_t} t_i^d\delta u_i dS = R_3 \tag{29}$$

$$\int_{\Omega} d_i\delta\phi_{,i}d\Omega - \int_{\partial\Omega_D} D_n^d\delta\phi dS = R_4 \tag{30}$$

The problem is completed with boundary conditions:

$$\phi = \phi^d \text{ on } \partial\Omega_\phi \tag{31}$$

$$d_i n_i = -D_n^d \text{ on } \partial\Omega_D \tag{32}$$

$$u_i = u^d \text{ on } \partial\Omega_u \tag{33}$$

$$t_k = n_j\left(\sigma_{jk} - \tau_{ijk,i}\right) - D_j\left(n_i\tau_{ijk}\right) = t_k^d \text{ on } \partial\Omega_t \tag{34}$$

$$u_{i,j}n_j = v_i^d \text{ on } \partial\Omega_v \tag{35}$$

$$n_i n_j\tau_{ijk} = r_k^d \text{ on } \partial\Omega_r \tag{36}$$

where ϕ^d, D_n^d, $\mathbf{u}^d$, $\mathbf{t}^d$, $\mathbf{v}^d$ and $\mathbf{r}_k^d$ are the prescribed electric potential, surface charge density, displacements, tractions, normal derivative of the displacement and the higher-order traction, respectively. $\mathbf{n}$ is the unitary normal vector to the boundary $\partial\Omega$ and $D_j(.) = \frac{\partial(.)}{\partial x_j} - n_j n_q \frac{\partial(.)}{\partial x_q}$. Here, we assume $\mathbf{v}^d = \mathbf{r}_k^d = 0$ on $\partial\Omega_v$ and $\partial\Omega_r$.

IV. IGA DISCRETIZATION OF DYNAMIC EQUATIONS

The key idea of isogeometric analysis is to unify the geometry and analysis models[? ?]. The NURBS basis functions with higher continuity are employed to solve the fourth order flexoelectric PDEs. The basis function for NURBS surfaces is defined as:

$$R_{i,j}^{p,q}(\xi,\eta) = \frac{N_{i,p}(\xi)M_{j,q}(\eta)w_{i,j}}{\sum_{\hat{i}=1}^{n}\sum_{\hat{j}=1}^{m}N_{\hat{i},p}(\xi)M_{\hat{j},q}(\eta)w_{\hat{i},\hat{j}}} \tag{37}$$

where the knots $\boldsymbol{\xi} = \{\xi_1, \xi_2, ..., \xi_{n+p+1}\}$, $\boldsymbol{\eta} = \{\eta_1, \eta_2, ..., \eta_{m+q+1}\}$. p and q are the polynomial order. n and m are the number of basis function, $w_{i,j}$ are positive weights. $N_{i,p}(\xi)$ and $M_{i,q}(\eta)$ are univariate B-Spline basis of order p and q corresponding to knot vectors $\boldsymbol{\xi}$ and $\boldsymbol{\eta}$, respectively, and are recursively defined as[?]

$$N_{i,0} = \begin{cases} 0, & if\ \xi_i \le \xi \le \xi_{i+1} \\ 1, & otherwise. \end{cases} \tag{38}$$

and for $p = 1, 2, ...$, we have

$$N_{i,p}(\xi) = \frac{\xi - \xi_i}{\xi_{i+p} - \xi_i}N_{i,p-1}(\xi) + \frac{\xi_{i+p+1} - \xi}{\xi_{i+p+1} - \xi_{i+1}}N_{i+1,p-1}(\xi) \tag{39}$$

The displacement $\mathbf{u}$ and electric potential ϕ fields are approximated by

$$\mathbf{u}(\mathbf{x}) = \sum_{i=1}^{n}\sum_{j=1}^{m}R_{i,j}^{p,q}(\xi,\eta)u_{ij}^e = \boldsymbol{N}_u\boldsymbol{u}^e \tag{40}$$

$$\phi(\mathbf{x}) = \sum_{i=1}^{n}\sum_{j=1}^{m}R_{i,j}^{p,q}(\xi,\eta)\phi^e = \boldsymbol{N}_\phi\boldsymbol{\phi}^e \tag{41}$$

and their derivatives are given by

$$\boldsymbol{\varepsilon} = \boldsymbol{B}_u\boldsymbol{u}^e,\ \ \boldsymbol{E} = -\boldsymbol{B}_\phi\boldsymbol{\phi}^e,\ \ \boldsymbol{u}_{,jk} = \boldsymbol{H}_u\boldsymbol{u}^e \tag{42}$$

For the open circuit condition, substituting (**??**)-(**??**) to (**??**)-(**??**), then the discrete dynamic electromechanical system can be obtained as

$$\begin{cases} \mathbf{M}\ddot{\mathbf{u}} + \mathbf{D}\dot{\mathbf{u}} + \mathbf{K}_{uu}\mathbf{u} + \mathbf{K}_{\phi u}^T\boldsymbol{\phi} = \mathbf{f}_u \\ \qquad \mathbf{K}_{\phi u}\mathbf{u} + \mathbf{K}_{\phi\phi}\boldsymbol{\phi} = \mathbf{f}_\phi \end{cases} \tag{43}$$

and

$$\mathbf{K}_{uu} = \sum_e \int_{\Omega_e} [\boldsymbol{B}_u^T \mathbf{C} \boldsymbol{B}_u + \boldsymbol{H}_u^T \mathbf{G} \boldsymbol{H}_u] d\Omega \tag{44}$$

$$\mathbf{K}_{\phi u} = \sum_e \int_{\Omega_e} [\boldsymbol{B}_\phi^T \mathbf{e} \boldsymbol{B}_u + \boldsymbol{B}_\phi^T \boldsymbol{\mu} \boldsymbol{H}_u] d\Omega \tag{45}$$

$$\mathbf{K}_{\phi\phi} = -\sum_e \int_{\Omega_e} [\boldsymbol{B}_\phi^T \boldsymbol{\alpha} \boldsymbol{B}_\phi] d\Omega \tag{46}$$

$$\mathbf{M} = \sum_e \int_{\Omega_e} \rho_0 \{\boldsymbol{N}^T \boldsymbol{N} + \ell_d^2 \tilde{\boldsymbol{B}}_u^T \tilde{\boldsymbol{B}}_u\} d\Omega \tag{47}$$

$$\mathbf{D} = \beta_1 \mathbf{M} + \beta_2 \mathbf{K}_{uu} \tag{48}$$

$$\mathbf{f}_u = \int_\Omega \mathbf{N}_u^T \mathbf{t}^d d\Omega \tag{49}$$

$$\mathbf{f}_\phi = -\int_\Omega \mathbf{N}_\phi^T D_n^d d\Omega \tag{50}$$

where $\mathbf{M}$ is mass matrix and $\mathbf{D}$ is Rayleigh damping matrix. B_ϕ, B_u and H_u are the matrices containing the gradient and Hessian of the corresponding basis functions N_ϕ and N_u which are defined in Appendix.**??**. The matrix forms of the stiffness tensor C_{ijkl}, dielectric tensor α_{ij}, flexoelectric tensor μ_{ijkl} and strain-gradient tensor G_{ijklmn} are given in Appendix.**??**. β_1 and β_2 are constants of proportionality calculated by two damping ratios ξ_1 and ξ_2, as well as the first two resonance frequencies of the structure ω_1 and ω_2,

$$\begin{bmatrix} \beta_1 \\ \beta_2 \end{bmatrix} = \frac{2\omega_1\omega_2}{\omega_1^2 - \omega_2^2} \begin{bmatrix} -\omega_2 & \omega_1 \\ \frac{1}{\omega_2} & -\frac{1}{\omega_1} \end{bmatrix} \begin{bmatrix} \xi_1 \\ \xi_2 \end{bmatrix} \tag{51}$$

The external vibration and the steady state response are assumed harmonic form with the same frequency,

$$\mathbf{f}_u = \mathbf{F}_u e^{j\omega t},\ \mathbf{f}_\phi = \mathbf{F}_\phi e^{j\omega t},\ \mathbf{u} = \mathbf{U} e^{j\omega t},\ \phi = \mathbf{\Phi} e^{j\omega t} \tag{52}$$

Substituting (**??**) into (**??**), the coupling governing equations can be obtained in frequency domain

$$\begin{bmatrix} \mathbf{K}_{uu} + j\omega\mathbf{D} - \omega^2\mathbf{M} & \mathbf{K}_{\phi u}^T \\ \mathbf{K}_{\phi u} & \mathbf{K}_{\phi\phi} \end{bmatrix} \begin{bmatrix} \mathbf{U} \\ \mathbf{\Phi} \end{bmatrix} = \begin{bmatrix} \mathbf{F}_u \\ \mathbf{F}_\phi \end{bmatrix} \tag{53}$$

V. TOPOLOGY OPTIMIZATION OF FLEXOELECTRIC MICRO AND MACRO STRUCTURES

In this work, we propose a two-scale topology optimization of an electromechanical energy harvester made of non-piezoelectric material. At the microscale (see Fig. **??** (a)), the periodic mi-

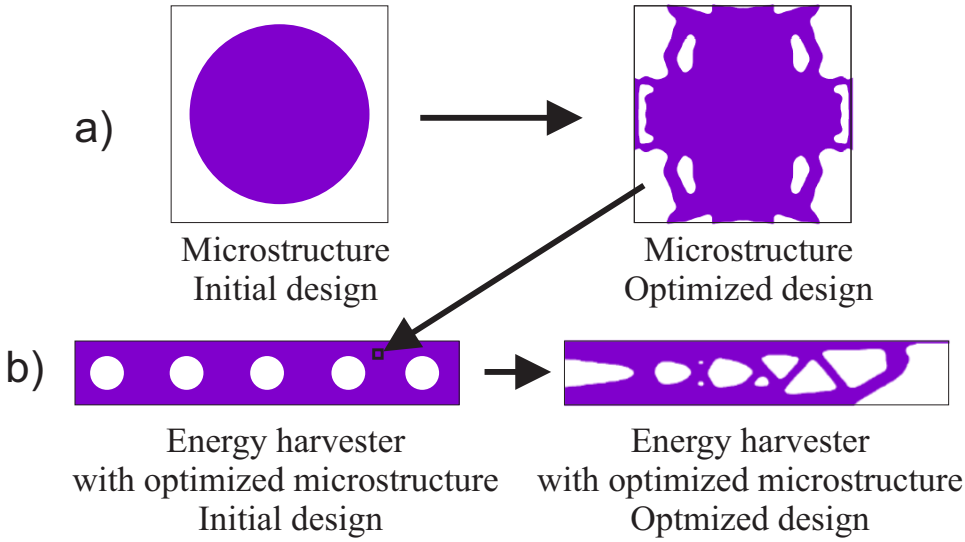

FIG. 2: Multiscale topology optimization strategy for the design of the electromechanical energy harvester made of a non-piezoelectric material: (a) micro scale topology optimization problem; (b) macro scale topology optimization problem

crostructure of the material is optimized to maximize its flexoelectric effective properties. Then, homogenization is performed to obtain the corresponding coefficient of the macroscopic electromechanical properties. At the structural level (macro scale, see Fig. **??** (b)), a second topology optimization step is performed to maximize the electromechanical coupling factor (ECF) of the harvester under dynamic conditions. The overall procedure is summarized in Fig. **??**.

A. SIMP framework with IGA

A SIMP[? ?] Topology Optimization is adopted, where the geometry is defined within a design domain by means of densities ρ defined over the nodes of a mesh. In the present work, an Isogeometric Analysis (IGA) scheme is used both for solving equilibrium equations at micro and macro scales, but also to define the interpolation of densities within the Topology Optimization scheme[? ?] . The main advantage of IGA in the present framework is to allow C^1 continuity, which is required to solve the equations of the strain -gradient flexoelectric problems at both micro and macro scales. A complete description of the IGA discretization scheme which is used in this work can be found in our previous paper[?] . The density design variables are defined on control points, i.e. nodal densities. These densities are used to interpolate the material properties in a continuous manner, using penalty exponents to enforce local densities to values close to 0 or 1. In SIMP, the

material properties are interpolated as follows, where the elastic tensor is taken as illustration:

$$C_{ijkl}(\rho) = C^{min}_{ijkl} + \rho^{p_c}(C^{0}_{ijkl} - C^{min}_{ijkl}) \tag{54}$$

where C^{min}_{ijkl} are small numerical values associated with void (no material). The same interpolation scheme is used to interpolate the other material tensors, at both micro and macro scales. The coefficients p_c is a numerical penalty exponent. The penalty corresponding to the interpolation of piezoelectric, flexoelectric and dielectric properties are denoted by p_e, p_μ, p_a, respectively. Different coefficients can be used for the other material properties.

B. Microstructure topology optimization problem

At the micro scale, the objective is to obtain the largest effective flexoelectric coefficients by designing the microstructure of the periodic flexoelectric composites. The topology optimization problem is then formulated so as to maximize one specific component of the effective flexoelectric tensor in (**??**).

$$\begin{aligned} &\underset{\rho}{\text{Max}} : \ \overline{\mu}_{ijkl} \\ &\text{Subject to} : \begin{cases} R_1(\rho) = 0 \\ R_2(\rho) = 0 \\ \int_{\Omega_m} \rho dV \leq f^m \\ 0 \leq \rho \leq 1, \end{cases} \end{aligned} \tag{55}$$

where f^m is the micro volume fraction constraint, or density of the material.

C. Macroscopic dynamic electromechanical topology optimization

Once the microstructure is optimized from the previous section description, the obtained homogenized properties (see**?** to obtain a detailed description of the expression of the homogenized tensors) are used as material properties in the macro equations describing the behavior of the energy harverster in Eqs. (**??**)-(**??**), (**??**)-(**??**). Then, a second Topology Optimization step is performed at the macro structural level. Here, the objective is to maximize the dynamic electromechanical response of the structure. More specifically, the electromechanical coupling factor

(ECF) of an electromechanical systems under harmonic excitation for a given frequency is defined as:

$$k_{eff}^2 = \frac{\Pi_e(\omega)}{\Pi_m(\omega)} \tag{56}$$

$$\Pi_e(\omega) = \frac{1}{2}\int_\Omega E_i^*(\omega)\bar{\alpha}_{ij}E_j(\omega) \tag{57}$$

$$\Pi_m(\omega) = \frac{1}{2}\int_\Omega \varepsilon_{ij}^*(\omega)\bar{C}_{ijkl}\varepsilon_{kl}(\omega) \tag{58}$$

where the $\Pi_e(\omega)$ and $\Pi_m(\omega)$ are electric and mechanical energies, respectively, and $E_i^* = -\phi_{,i}^*$, with ϕ^* is the complex conjugate to ϕ, and $\varepsilon_{ij}^* = -\nabla_i^s u_j^*$, with u_j^* is the complex conjugate to u_j.

The topology optimization problem is formulated so as maximizing the ECF k_{eff}^2 at a given excitation frequency, under volume and compliance constraints:

$$\begin{aligned} &\underset{\rho}{\text{Min}}: \; J(\rho) = \tfrac{1}{k_{eff}^2(\rho)} = \tfrac{\Pi_m(\omega,\rho)}{\Pi_e(\omega,\rho)} \\ &\text{Subject to}: \begin{cases} \int_{\Omega_M}\rho dV \le \frac{V^{max}}{V^0} \\ R_3(\rho) = 0 \\ R_4(\rho) = 0 \\ \hat{C}(\rho) \le \hat{C}^{max} \\ 0 \le \rho \le 1, \end{cases} \end{aligned} \tag{59}$$

In the above, V^0 is the design domain volume and V^{max} is the maximum volume of the structure. In Eq. (**??**), $\hat{C}(\rho) = \Pi_m(0)$ is the static average compliance, which it is expected to eliminate disconnected domain by ensuring a minimal stiffness to the structure. The micro and macro optimization problems in (**??**) and (**??**) are solved by the conservative convex separable approximations (CCSAs) optimizer[**?**] based on the adjoint sensitivity (detailed sensitivity analysis in Appendix.**??**).

VI. APPLICATIONS

In the following examples, we first design the microstructure of a periodic porous material made of a non-piezoelectric material, but possessing flexoelectric behavior, so as to maximize its apparent flexoelectric properties. The resulting material has homogenized (apparent) non-zero piezoelectric properties. In a second step, we optimize the design of structures serving as energy harvesters in a dynamic regime and made with this material. The objective is to show that energy

harvesters using electromechanical transduction can be designed using fully non-piezoelectric materials. The polynomial orders of NURBS mesh are chosen as $p = q = 3$ for all cases.

A. Topology optimization of a non-piezoelectric microstructure made of a flexoelectric material

We first conduct the Topology Optimization (TO) of a microstructure made of a non-piezoelectric material, but having flexoelectric behavior. Since the energy harvester structures considered in this work mainly involve bending, we perform the TO of the microstructure so as to maximize the effective flexoelectric coefficient μ_{2112}, which characterizes the polarization under bending. The flexoelectric microstructure is made of centrosymmetric flexoelectric (non-piezoelectric) material $SrTiO_3$ (STO), whose parameters are given in Table **??**. The second phase is void (air). For this material, $\mu_{2112} \equiv \mu_{12} = 7$ nC/m and here, all penalty exponents used in the TO numerical procedure (see Eq. (**??**)) are chosen as equal to 3.

TABLE I: Material properties of $SrTiO_3$ (STO)[? ?]

Density	Elastic coefficients	Dielectric coefficients	Flexoelectric coefficients
$\rho_0 = 5.12\text{g/cm}^3$	$c_{11} = c_{22} = 319$ GPa	$\alpha_{11} = 300\varepsilon_0$	$\mu_{11} = 0.2$ nC/m
	$c_{12} = 100$ GPa	$\alpha_{33} = 300\varepsilon_0$	$\mu_{12} = 7$ nC/m
	$c_{44} = 110$ GPa	$\varepsilon_0 = 8.854 \times 10^{-12}$C/V. m	$\mu_{44} = 5.8$ nC/m

The microstructural optimized topologies are provided for different volume fractions in Fig. **??**. The optimized values of the flexoelectric component $\bar{\mu}_{2112}$ corresponding to the volume fractions f_1 =0.5, f_2 =0.6, f_3 =0.7 and f_4 =0.8 are respectively obtained as 7.14 nC/m, 9.19 nC/m, 10.10 nC/m and 12.15 nC/m, which represent a significant improvement as compared to STO of 2.00%, 31.29%, 44.29% and 73.57%, respectively. Note that even though non-piezoelectric, the material with optimized microstructure actually exhibits an apparent piezoelectric behavior due to local flexoelectricity. The respective values of the effective piezoelectric coefficient $\bar{e}_{211}$ corresponding to the volume fractions f_1, f_2, f_3 and f_4 are respectively obtained as 0.0032 nC/m^2, -0.0850 nC/m^2, -0.0201 nC/m^2, 0.3061 nC/m^2 . The piezoelectric coefficients $\bar{e}_{111}$, $\bar{e}_{211}$ and $\bar{e}_{222}$ of the microstructures for the different volume fractions are summarized in Table **??**.

In the following, we will use the optimized microstructure corresponding to the volume frac-

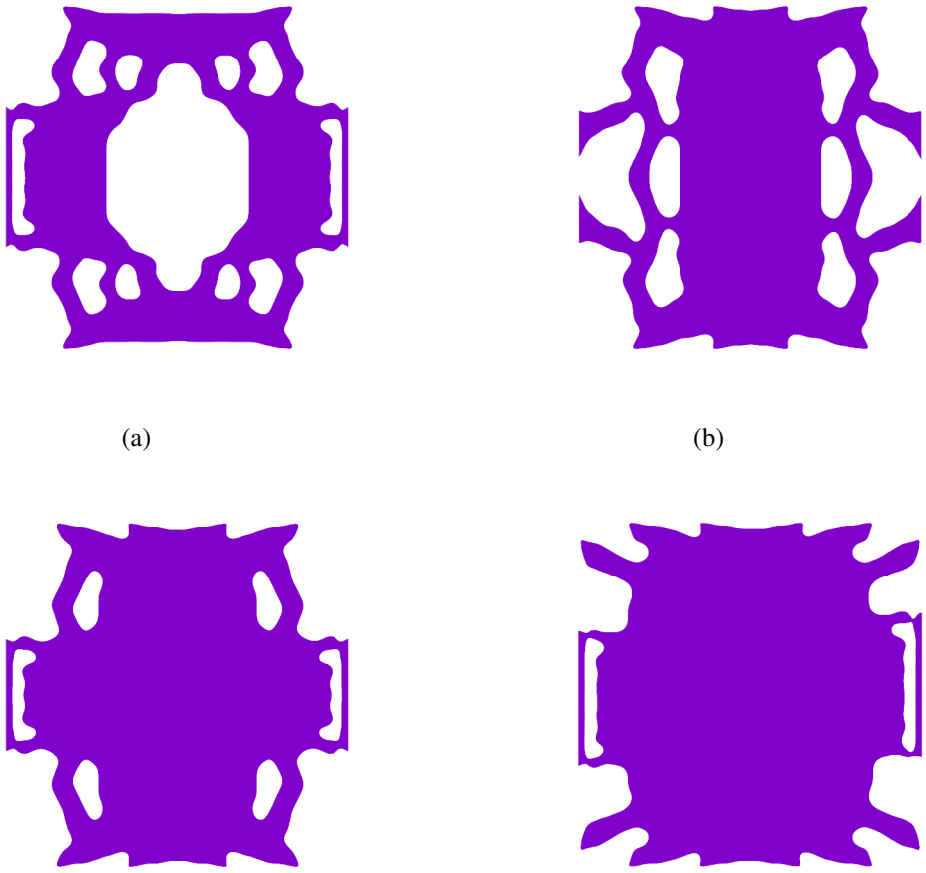

(a) (b)

(c) (d)

FIG. 3: Optimized microstructure with respect to the apparent flexoelectric coefficient $\bar{\mu}_{2112}$ for different volume fractions: (a) $f_1 = 0.5$; (b) $f_2 = 0.6$; (c) $f_3 = 0.7$; (d) $f_4 = 0.8$.

tion $f_4 = 0.8$ (see Fig.**??**) as a constitutive material for energy harvesters designs. The effective parameters corresponding to this optimized microstructure are provided in Eqs. (**??**)-(**??**). Note that such microstructures are complex, but may be fabricated with the recent advances in additive manufacturing, including 3D printing of ceramics (see e.g.[**?**]).

$$\mathbf{C} = \begin{bmatrix} 72.83 & 22.68 & 0 \\ 22.68 & 103.21 & 0 \\ 0 & 0 & 29.91 \end{bmatrix} (GPa), \quad \boldsymbol{\alpha} = \begin{bmatrix} 0.804 & 0 \\ 0 & 1.121 \end{bmatrix} (nC/V \cdot m) \tag{60}$$

TABLE II: Piezoelectric coefficients $\bar{e}_{111}$, $\bar{e}_{211}$ and $\bar{e}_{222}$ (unit: nC/m^2) of microstructures with different volume fractions

Volume fraction	$\bar{e}_{111}$	$\bar{e}_{211}$	$\bar{e}_{222}$
f_1 =0.5	0.0163	0.0032	-0.0271
f_2 =0.6	-0.4471	-0.0850	-0.1472
f_3 =0.7	0.0318	-0.0201	-0.0584
f_4 =0.8	-0.0209	0.3061	0.1456

$$\boldsymbol{e} = \begin{bmatrix} -0.0209 & 0.0512 & -0.0697 \\ 0.3061 & 0.1456 & -0.0608 \end{bmatrix} (nC/m^2) \tag{61}$$

$$\boldsymbol{\mu} = \begin{bmatrix} -0.16 & -0.18 & 0.64 & 0.06 & -0.05 & 2.38 \\ 0.07 & 12.15 & -0.05 & 1.37 & 0.62 & -0.05 \end{bmatrix} (nC/m) \tag{62}$$

B. Design of a dynamic beam-like energy harvester

In this example, we use the proposed methodology to design a dynamic beam-like energy harvester in open circuits boundary condition as shown as Fig.**??**. The beam material is the one obtained from the optimized microstructure in the previous section, whose coefficients are provided in (**??**)-(**??**). The size of the beam is $h = 200$ nm, with an aspect ratio $L/h = 6$. The density of the optimized microstructure is $\rho_0 = 4.096 g/cm^3$. The internal length scale of higher-order elastic tensor (**??**) is $\ell = 1 \times 10^{-8}$ m**?** . Askes et al**?** suggested that the micro inertial length should be $\ell_d > \ell$. The author**?** also observed a good agreement between the gradient elasticity model and wave dispersion results of carbon nanotubes based on molecular dynamics (MD) obtained by Wang et al**?** , when ℓ_d is in the range 3ℓ - 35ℓ. Here, we choose micro inertial length in Eq. (**??**) as $\ell_d = 10\ell$. The influence of micro inertial length on the numerical results of electromechanical coupling factors and resonance frequency was investigated in**?** . The modal damping ratios (see**?**) are taken as $\xi_1 = \xi_2 = 0.01$. The excitation frequency is $F(\omega) = F_0 e^{j\omega t}$ and $F_0 = -1$ N, applied along the x_2-direction on the top-right corner. The dynamic topology optimization is carried out for the excitation frequencies 0 MHz (static), 10 MHz, 12 MHz, 15 MHz and 16 MHz.

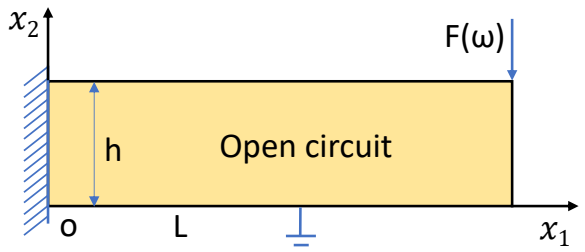

FIG. 4: Beam-like energy harverster with open circuit boundary conditions: design domain

The volume fraction constraint, defined as the quantity of material as compared to the design domain volume $L \times h$ is set as f =0.6 for all frequency cases. The compliance constraint is set as $\hat{C}^{max} = 8\overline{\Pi}_1(0)$, where $\overline{\Pi}_1(0)$ is the static strain energy of the undesigned flexoelectric beam. Here the undesigned structure means that the relative densities in the whole rectangular design domain are equal to 1. For comparison, a guess design consisting into a rectangular beam with 6 holes as depicted in Fig.**??**(a)) is analyzed. The holes radii are $R = 0.3568h$ corresponding to a volume fraction equal to 0.6. This structure will serve as a reference to be compared with the optimized designs. The penalty exponents used in the TO numerical procedure (see Eqs. (**??**)) are chosen here as $p_c = p_e = 3,\ p_a = 1$. These coefficients are different in this example for convergence reasons. This combination of penalty exponents means that the mechanical and electromechanical stiffness are penalized to make the optimal solution converge to 1 or 0, while the dielectric one is interpolated by a linear material model.

The dynamic topology optimization of the flexoelectric cantilever beam is performed for different excitation frequencies. Initialization of the densities is performed by setting them uniformly to $\rho_e = 0.6$ in the rectangular design domain defined in Fig. **??**. The final optimized geometries, obtained respectively for the excitation frequencies 0 MHz, 10 MHz, 12 MHz, 15 MHz and 16 MHz, are depicted in Fig. **??**. The corresponding electromechanical coupling factors (ECFs) are listed in Table **??**. The ECFs of the optimized structures for excitation frequencies 0 MHz, 10 MHz, 12 MHz, 15 MHz and 16 MHz increase by factors of 20.18, 20.07, 20.04, 19.99 and 19.97 times, respectively, as compared to the reference design in Fig.**??**(a).

The ECF frequency responses for the optimized geometries are compared to the reference response in Fig.**??**, where the frequency ranges from 0 to 143 MHz. It is observed that the ECF frequency responses of all optimal designs obtained by different excitation frequencies are much

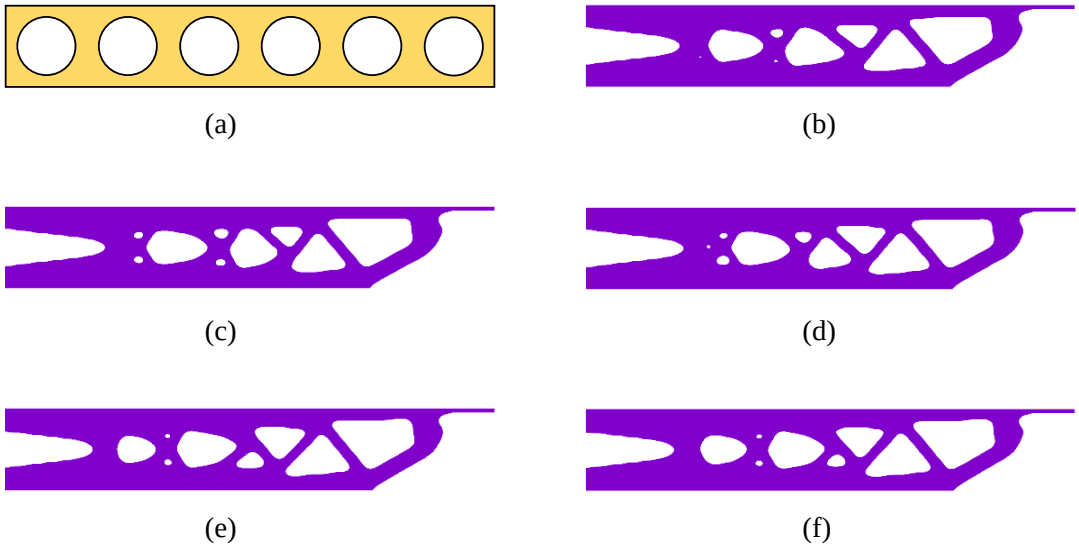

FIG. 5: (a) Reference design for the beam-like energy harvester; Optimized design corresponding to excitation frequencies: (b) Static conditions; (c) 10 MHz; (d) 12 MHz; (e) 15 MHz; (f) 16 MHz

larger (about 20 times) than the reference in a large frequency range (roughly between 0 and 100 MHz), while it drops for frequencies larger than 100 MHz. Using different excitation frequencies in the topology optimization does not modify significantly the ECF response of the optimized structure. In conclusion, it is shown that the obtained optimized energy harvester structures have good performances both with respect to the reference (guess design) and considering that the constitutive material is not piezoelectric.

TABLE III: electromechanical coupling factors (ECF) of optimal designs for flexoelectric nano beam under different excitation frequencies

Excitation Frequency	ECF (optimized)	ECF (reference)	Gain: ECF_{opt}/ECF_{ref}
0 MHz	0.03420	1.6149×10^{-3}	21.18
10 MHz	0.03406	1.6165×10^{-3}	21.07
12 MHz	0.03402	1.6171×10^{-3}	21.04
15 MHz	0.03397	1.6184×10^{-3}	20.99
16 MHz	0.03395	1.6189×10^{-3}	20.97

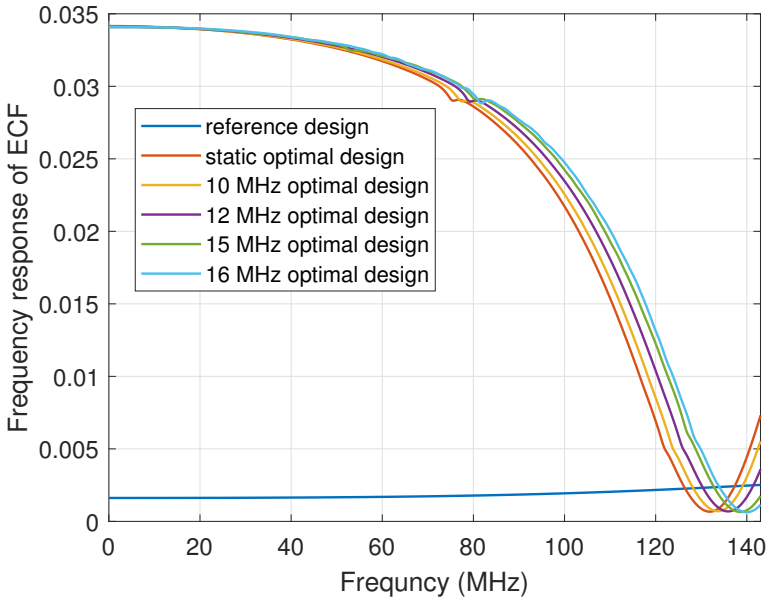

FIG. 6: ECF frequency responses of reference and optimized designs for flexoelectric beam for different excitation frequencies

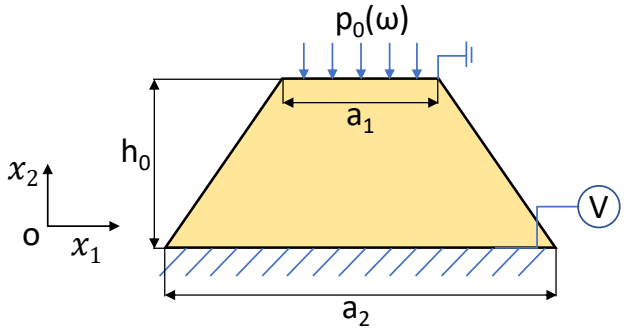

FIG. 7: Energy harvester with truncated pyramid-shape under compression and open circuit conditions: design domain

C. Design of dynamic truncated pyramid-like energy harvester

In this example, we consider the design of an energy harvester with truncated pyramid shape and open circuit conditions, as shown in Fig.**??**. This shape is often chosen in flexoelectric systems as inducing strain gradient in compression**?** . The initial design domain is defined by the geometrical parameters $a_1 = 400$ nm, $a_2 = 1200$ nm and $h_0 = 400$ nm. A spatially uniform and

oscillating pressure $p_0(\omega) = -1e^{j\omega t}$ N is applied on the top surface along the x_2-direction and the displacement DOFs on the bottom surface are fixed. The material parameters and length scale ℓ, ℓ_d are same as in the previous example. The volume fraction constraint is here set as $f = 0.7$. The compliance constraint is set as $\hat{C}^{max} = 4\overline{\Pi}_2(0)$, where $\overline{\Pi}_2(0)$ is the static strain energy of the truncated pyramid design domain with $\rho = 1$. A reference guess design is defined in Fig.**??**(a), consisting into a truncated pyramid including a circular void with radius $R' = 0.437h_0$. The penalty exponents used in the numerical TO procedure (see Eqs. (**??**)) are chosen as $p_c = p_e = 3,\ p_a = 1$.

We perform the topology optimization of the flexoelectric truncated pyramid under the excitation frequencies 0 MHz (static), 200 MHz, 600 MHz, 800 MHz and 1000 MHz. The final optimized structures obtained for the excitation frequencies mentioned above are presented in Fig.**??**. We can see that the vertical lengths of the voids in the topologies of the optimized structures become shorter and the material is concentrated more towards the middle domain of the structures, with the increasing frequencies of excitation in optimization. The ECFs of the reference and optimized structures are summarized in Table **??**. The ECFs of the optimized structures designed for excitation frequencies 0 MHz, 200 MHz, 600 MHz, 800 MHz and 1000 MHz increase respectively by 4.044, 3.293, 2.846, 2.403 and 2.089 times with respect to the reference design solutions. The ECFs frequency responses of reference structure and optimized designs obtained for the different excitation frequencies are shown in Fig.**??**, where the frequency ranges from 0 to 3.16 GHz. Obviously, the ECF is improved by the optimized energy harvester as compared to the reference design, and this for the whole frequency range. As another observation, the designs obtained by the dynamic topology optimization (taking into account nonzero excitation frequencies), mainly improves the ECF as compared to the ones obtained by static TO. Finally, it seems that increasing the excitation frequency decreases the ECF at low frequencies, but for larger frequencies there is not clear trend. Globally, the dynamic TO leads to a clear ECF improvement as compared to the reference of static designs, showing the potential of this framework.

VII. CONCLUSIONS

In this work, an innovative multiscale topology optimization approach was presented for the design of electromechanical energy harvesting systems using non-piezoelectric materials. The microscopic scale optimization focuses on maximizing the effective flexoelectric properties of a periodic, porous, and flexoelectric material. This leads to an effective material with apparent

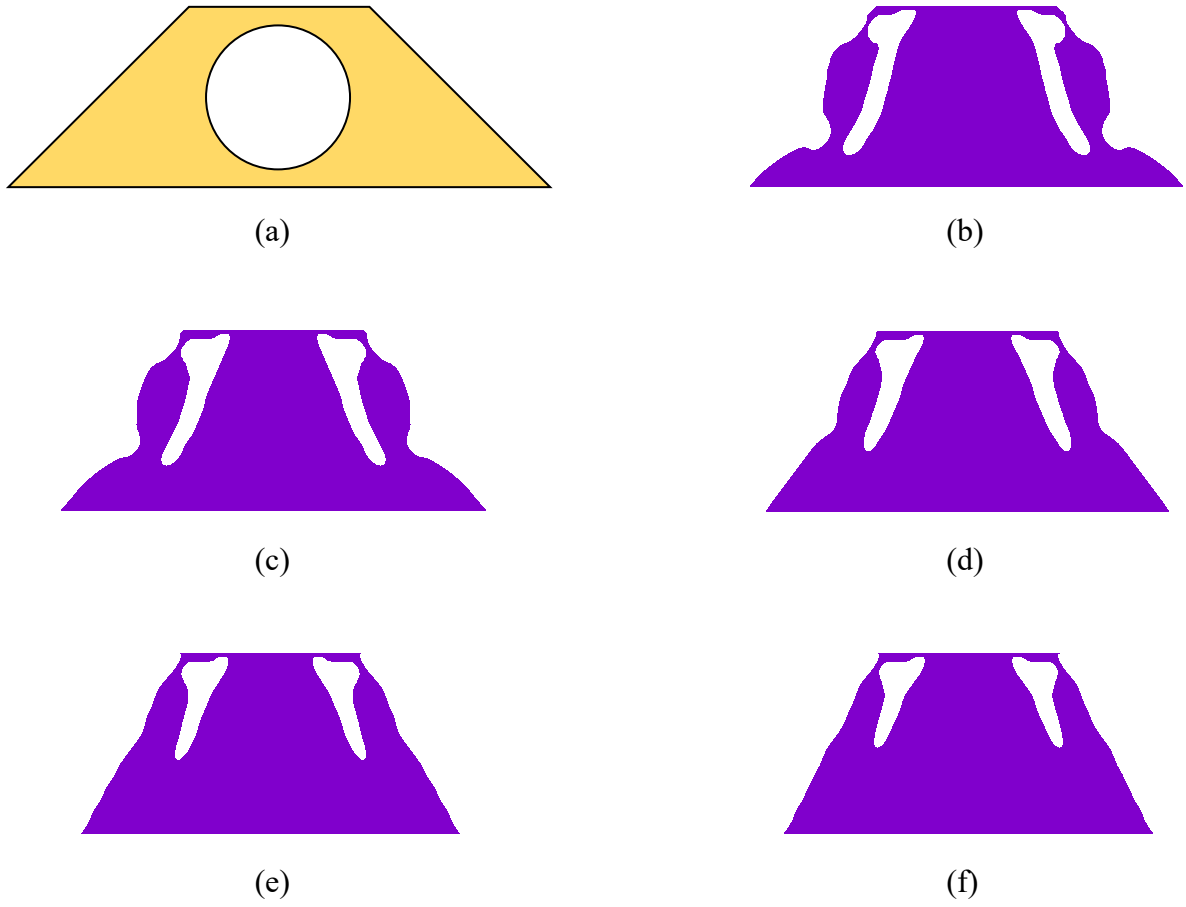

FIG. 8: (a) Reference design for the truncated pyramid-like energy harvester; Optimized design corresponding to excitation frequencies: (b) Static conditions; (c) 200 MHz; (d) 600 MHz; (e) 800 MHz; (f) 1000 MHz

piezoelectric properties, achieved without the use of piezoelectric materials. Subsequently, at the structure scale, a second topology optimization step is performed to maximize the Electromechanical Coupling Factor (ECF) for a specified forced vibration frequency. The optimized structures demonstrate significant improvements in ECF, ranging between 2 and 20 times, as compared to non-optimized structures of same volume across various excitation frequencies.

This approach opens up new possibilities for the design of energy harvesting systems, without the need for piezoelectric materials. The future implications of this research lie in the development of new micro- and nanoscale energy harvesting systems, potentially using new sources of materials and exploiting the potential of microstructure modifications to optimize their performance.

TABLE IV: electromechanical coupling factors (ECF) of optimized designs for truncated pyramid obtained by different excitation frequencies

Excitation Frequency	ECF (optimized)	ECF (reference)	Gain: ECF_{opt}/ECF_{ref}
0 MHz	7.4203×10^{-3}	1.4712×10^{-3}	5.044
200 MHz	6.3395×10^{-3}	1.4766×10^{-3}	4.293
600 MHz	5.9021×10^{-3}	1.5346×10^{-3}	3.846
800 MHz	5.4302×10^{-3}	1.5956×10^{-3}	3.403
1000 MHz	5.2058×10^{-3}	1.6852×10^{-3}	3.089

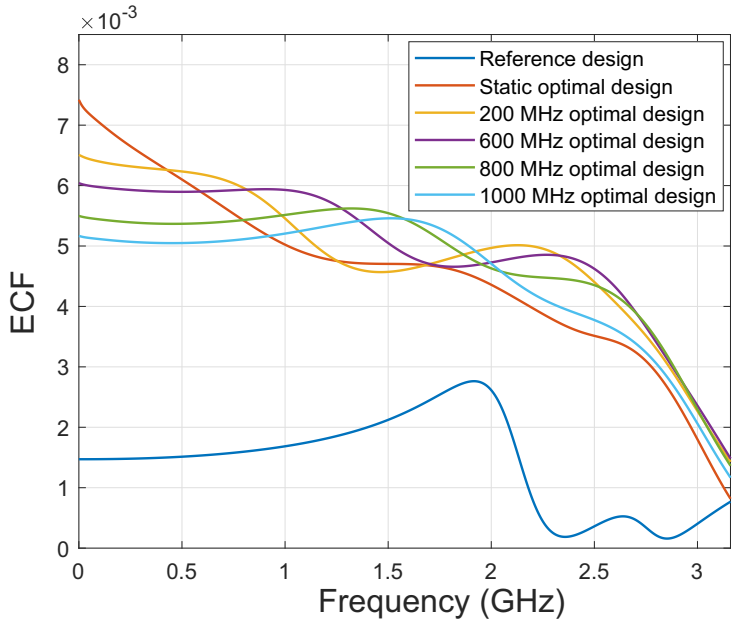

FIG. 9: ECF frequency responses of reference and optimized designs for truncated pyramid for different excitation frequencies

VIII. ACKNOWLEDGMENTS

Xing Chen acknowledges the support from China Scholarship Council (CSC No. 202106370116)

IX. CONFLICT OF INTEREST STATEMENT

On behalf of all authors, the corresponding author states that there is no conflict of interest.

X. REPLICATION OF RESULTS

Results can be made available on reasonable request to the corresponding author.

Appendix A: Matrices of material and IGA discretization

B_ϕ, B_u and H_u are the matrices containing the gradient and Hessian of the corresponding basis functions N_ϕ and N_u which are given by

$$\boldsymbol{B}_\phi = \begin{bmatrix} \frac{\partial N_1}{\partial x} & \cdots & \frac{\partial N_n}{\partial x} \\ \frac{\partial N_1}{\partial y} & \cdots & \frac{\partial N_n}{\partial y} \end{bmatrix}, \; \boldsymbol{B}_u = \begin{bmatrix} \frac{\partial N_1}{\partial x} & \cdots & \frac{\partial N_n}{\partial x} & 0 & \cdots, & 0 \\ 0 & \cdots & 0 & \frac{\partial N_1}{\partial y} & \cdots & \frac{\partial N_n}{\partial y} \\ \frac{\partial N_1}{\partial y} & \cdots & \frac{\partial N_n}{\partial y} & \frac{\partial N_1}{\partial x} & \cdots & \frac{\partial N_n}{\partial x} \end{bmatrix} \tag{A1}$$

$$\tilde{\boldsymbol{B}}_u = \begin{bmatrix} \frac{\partial N_1}{\partial x} & \cdots & \frac{\partial N_n}{\partial x} & 0 & \cdots, & 0 \\ 0 & \cdots & 0 & \frac{\partial N_1}{\partial y} & \cdots & \frac{\partial N_n}{\partial y} \\ \frac{\partial N_1}{\partial y} & \cdots & \frac{\partial N_n}{\partial y} & 0 & \cdots & 0 \\ 0 & \cdots & 0 & \frac{\partial N_1}{\partial x} & \cdots & \frac{\partial N_n}{\partial x} \end{bmatrix}, \; \boldsymbol{H}_u = \begin{bmatrix} \frac{\partial^2 N_1}{\partial x^2} & \cdots & \frac{\partial^2 N_n}{\partial x^2} & 0 & \cdots & 0 \\ 0 & \cdots & 0 & \frac{\partial^2 N_1}{\partial y^2} & \cdots & \frac{\partial^2 N_n}{\partial y^2} \\ \frac{\partial^2 N_1}{\partial x \partial y} & \cdots & \frac{\partial^2 N_n}{\partial x \partial y} & 0 & \cdots & 0 \\ 0 & \cdots & 0 & \frac{\partial^2 N_1}{\partial x \partial y} & \cdots & \frac{\partial^2 N_n}{\partial x \partial y} \\ \frac{\partial^2 N_1}{\partial x \partial y} & \cdots & \frac{\partial^2 N_n}{\partial x \partial y} & \frac{\partial^2 N_1}{\partial x^2} & \cdots & \frac{\partial^2 N_n}{\partial x^2} \\ \frac{\partial^2 N_1}{\partial y^2} & \cdots & \frac{\partial^2 N_n}{\partial y^2} & \frac{\partial^2 N_1}{\partial x \partial y} & \cdots & \frac{\partial^2 N_n}{\partial x \partial y} \end{bmatrix} \tag{A2}$$

The material parameters $\mathbf{C}$, $\boldsymbol{\alpha}$, $\boldsymbol{e}$, $\boldsymbol{\mu}$ and $\mathbf{G}$ are defined in the 2D matrix form as

$$\mathbf{C} = \begin{bmatrix} c_{11} & c_{12} & 0 \\ c_{12} & c_{22} & 0 \\ 0 & 0 & c_{44} \end{bmatrix}, \; \boldsymbol{\alpha} = \begin{bmatrix} \alpha_{11} & 0 \\ 0 & \alpha_{33} \end{bmatrix}, \; \boldsymbol{e} = \begin{bmatrix} 0 & 0 & e_{15} \\ e_{13} & e_{33} & 0 \end{bmatrix} \tag{A3}$$

$$\boldsymbol{\mu} = \begin{bmatrix} \mu_{11} & 0 & 0 & \mu_{12} & 0 & \mu_{44} \\ 0 & \mu_{11} & \mu_{12} & 0 & \mu_{44} & 0 \end{bmatrix} \tag{A4}$$

$$\mathbf{G} = \ell^2 \begin{bmatrix} c_{11} & 0 & 0 & c_{12} & 0 & 0 \\ 0 & c_{11} & c_{12} & 0 & 0 & 0 \\ 0 & c_{12} & c_{11} & 0 & 0 & 0 \\ c_{12} & 0 & 0 & c_{11} & 0 & 0 \\ 0 & 0 & 0 & 0 & c_{44} & 0 \\ 0 & 0 & 0 & 0 & 0 & c_{44} \end{bmatrix} \tag{A5}$$

Appendix B: Calculation of effective flexoelectric tensor

The strain and electric fields solutions, strain gradient fields solutions of the problem (**??**) can be expressed as the functions of the effective strain, electric and strain gradient fields as

$$\varepsilon_{ij} = A^0_{ijpq}\overline{\varepsilon}_{pq} - B^0_{ijp}\overline{E}_p - A^1_{ijpqr}\overline{\nabla\varepsilon}_{pqr} \tag{B1}$$

$$E_i = D^0_{ipq}\overline{\varepsilon}_{pq} - h^0_{ip}\overline{E}_p - D^1_{ipqr}\overline{\nabla\varepsilon}_{pqr} \tag{B2}$$

$$\nabla\varepsilon_{ijk} = J^0_{ijkpq}\overline{\varepsilon}_{pq} - Q^0_{ijkp}\overline{E}_p - J^1_{ijkpqr}\overline{\nabla\varepsilon}_{pqr} \tag{B3}$$

We define the displacement and electric fields matrices:

$$\mathbf{U} = \{\mathbf{U}_\phi;\mathbf{U}_u\},\ \mathbf{V} = \{\mathbf{V}_\phi;\mathbf{V}_u\},\ \mathbf{W} = \{\mathbf{W}_\phi;\mathbf{W}_u\} \tag{B4}$$

$$\mathbf{U}_u = [\mathbf{u}^1,\mathbf{u}^2,\mathbf{u}^3],\ \mathbf{V}_u = [\mathbf{u}^4,\mathbf{u}^5],\ \mathbf{W}_u = [\mathbf{u}^6,\mathbf{u}^7,\mathbf{u}^8,\mathbf{u}^9,\mathbf{u}^{10},\mathbf{u}^{11}] \tag{B5}$$

$$\mathbf{U}_\phi = [\phi^1,\phi^2,\phi^3],\ \mathbf{V}_\phi = [\phi^4,\phi^5],\ \mathbf{W}_\phi = [\phi^6,\phi^7,\phi^8,\phi^9,\phi^{10},\phi^{11}] \tag{B6}$$

The displacement fields $\mathbf{u}^i$ and the electric fields ϕ^i are the vector columns containing respectively the nodal displacement and electric potentials solution of the localization problems Eqs.(**??**) with the boundary conditions described in Table **??**.

The matrices associated with the tensors A^0, B^0, A^1, D^0, A^0, h^0, D^1, J^0, Q^0 and J^1 in (**??**)-(**??**) can be computed according to

$$\mathbf{A}^0(x) = \mathbf{B}_u(x)\mathbf{U}_u, \quad \mathbf{B}^0(\mathbf{x}) = \mathbf{B}_u(x)\mathbf{V}_u, \quad \mathbf{A}^1(\mathbf{x}) = \mathbf{B}_u(\mathbf{x})\mathbf{W}_u; \tag{B7}$$

$$\mathbf{D}^0(x) = -\mathbf{B}_\phi(x)\mathbf{U}_\phi, \quad \mathbf{h}^0(x) = -\mathbf{B}_\phi(x)\mathbf{V}_\phi, \quad \mathbf{D}^1(x) = -\mathbf{B}_\phi(x)\mathbf{W}_\phi \tag{B8}$$

$$\mathbf{J}^0(x) = \mathbf{H}_u(x)\mathbf{U}_u, \quad \mathbf{Q}^0(x) = \mathbf{H}_u(x)\mathbf{V}_u, \quad \mathbf{J}^1(x) = \mathbf{H}_u(x)\mathbf{W}_u \tag{B9}$$

Substituting (**??**)-(**??**) into (**??**), we have the effective flexoelectric tensor in matrix form as

$$\overline{\boldsymbol{\mu}} = -\left\langle \mathbf{V}_u^T\mathbf{B}_u^T\mathbf{C}\mathbf{B}_u\mathbf{W}_u - \mathbf{V}_\phi^T\mathbf{B}_\phi^T\boldsymbol{\alpha}\mathbf{B}_\phi\mathbf{W}_\phi + \mathbf{V}_u^T\mathbf{H}_u^T\boldsymbol{\mu}\mathbf{B}_\phi\mathbf{W}_\phi + \mathbf{V}_\phi^T\mathbf{B}_\phi^T\boldsymbol{\mu}\mathbf{H}_u\mathbf{W}_u \right\rangle \tag{B10}$$

Appendix C: Sensitivity analysis

To solve the effective flexoelectric coefficients enhancement problemn (**??**) for microstructure and the electromechanical coupling efficiency optimization problem (**??**) for energy harvester based on the gradient-based mathematical programming method, The adjoint method is employed to derive both the numerical sensitivities.

Field	$(\overline{\varepsilon}_{11},\overline{\varepsilon}_{22},\overline{\varepsilon}_{12})$	$(\overline{E_1},\overline{E_2})$	$(\overline{\nabla\varepsilon}_{111},\overline{\nabla\varepsilon}_{221},\overline{\nabla\varepsilon}_{122},\overline{\nabla\varepsilon}_{222},\overline{\nabla\varepsilon}_{112},\overline{\nabla\varepsilon}_{121})$
$\mathbf{u}^1,\phi^1$	(1,0,0)	(0,0)	(0,0,0,0,0,0)
$\mathbf{u}^2,\phi^2$	(0,1,0)	(0,0)	(0,0,0,0,0,0)
$\mathbf{u}^3,\phi^3$	$(0,0,\frac{1}{2})$	(0,0)	(0,0,0,0,0,0)
$\mathbf{u}^4,\phi^4$	(0,0,0)	(1,0)	(0,0,0,0,0,0)
$\mathbf{u}^5,\phi^5$	(0,0,0)	(0,1)	(0,0,0,0,0,0)
$\mathbf{u}^6,\phi^6$	(0,0,0)	(0,0)	(1,0,0,0,0,0)
$\mathbf{u}^7,\phi^7$	(0,0,0)	(0,0)	(0,1,0,0,0,0)
$\mathbf{u}^8,\phi^8$	(0,0,0)	(0,0)	(0,0,1,0,0,0)
$\mathbf{u}^9,\phi^9$	(0,0,0)	(0,0)	(0,0,0,1,0,0)
$\mathbf{u}^{10},\phi^{10}$	(0,0,0)	(0,0)	(0,0,0,0,1,0)
$\mathbf{u}^{11},\phi^{11}$	(0,0,0)	(0,0)	(0,0,0,0,0,1)

TABLE V: Elementary solution corresponding to the prescribed macroscopic strain, electric potential and strain gradient components

1. Microstructure analysis

The effective flexoeletric tensor can be wirtten by compact form as

$$\overline{\boldsymbol{\mu}} = -\frac{1}{\Omega_m}\begin{bmatrix}\mathbf{V}_\phi\\ \mathbf{V}_u\end{bmatrix}^T\begin{bmatrix}\mathbf{K}_{\phi\phi} & \mathbf{K}_{\phi u}\\ \mathbf{K}_{\phi u}^T & \mathbf{K}_{uu}\end{bmatrix}\begin{bmatrix}\mathbf{W}_\phi\\ \mathbf{W}_u\end{bmatrix} \tag{C1}$$

We define

$$\mathbf{K}_G = \begin{bmatrix}\mathbf{K}_{\phi\phi} & \mathbf{K}_{\phi u}\\ \mathbf{K}_{\phi u}^T & \mathbf{K}_{uu}\end{bmatrix} \tag{C2}$$

By using the adjoint method, the corresponding Lagrangian L^m for the effective flexoelectric tensor components optimization problem (**??**) is formed by introducing adjoint vectors λ_1^m and λ_2^m as:

$$L^m = \overline{\boldsymbol{\mu}} - (\mathbf{V}^T\mathbf{K}_G - \mathbf{F}_V{}^T)\boldsymbol{\lambda}_1^m - (\boldsymbol{\lambda}_2^m)^T(\mathbf{K}_G\mathbf{W} - \mathbf{F}_W{}^T) \tag{C3}$$

Where $\mathbf{V}^T\mathbf{K}_G - \mathbf{F}_V{}^T = 0$ and $\mathbf{K}_G\mathbf{W} - \mathbf{F}_W{}^T = 0$ are the IGA discrete forms of (**??**) with boundary condition shown in Table.**??**, and they hold for arbitrary vectors λ_1^m and λ_2^m. Differentiating the

Lagrangian L^m with respect to the design variable ρ^m gives:

$$\frac{\partial L^m}{\partial \rho^m} = \frac{\partial \overline{\boldsymbol{\mu}}}{\partial \rho^m} - \frac{\partial (\mathbf{V}^T \mathbf{K}_G - \mathbf{F}_V{}^T)}{\partial \rho^m} \boldsymbol{\lambda}_1^m - (\boldsymbol{\lambda}_2^m)^T \frac{\partial (\mathbf{K}_G \mathbf{W} - \mathbf{F}_W{}^T)}{\partial \rho^m} \tag{C4}$$

We finally obtain the adjoint sensitivity of effective flexoelectric components with respect to the density as

$$\frac{\partial \overline{\boldsymbol{\mu}}}{\partial \rho^m} = \frac{1}{\Omega_m} \begin{bmatrix} \mathbf{V}_\phi \\ \mathbf{V}_u \end{bmatrix}^T \cdot \frac{\partial}{\partial \rho^m} \left(\begin{bmatrix} \mathbf{K}_{\phi\phi} & \mathbf{K}_{\phi u} \\ \mathbf{K}_{\phi u}^T & \mathbf{K}_{uu} \end{bmatrix} \right) \cdot \begin{bmatrix} \mathbf{W}_\phi \\ \mathbf{W}_u \end{bmatrix} \tag{C5}$$

2. Energy harvester analysis

For the energy harvester in dynamics, the first derivative of the objective function J with respect to the nodal design variable $\rho_{i,j}$ is calculated as

$$\frac{\partial J}{\partial \rho_{i,j}} = \frac{\frac{\partial \Pi_m}{\partial \rho_{i,j}} \Pi_e - \Pi_m \frac{\partial \Pi_e}{\partial \rho_{i,j}}}{\Pi_e^2} \tag{C6}$$

The terms $\frac{\partial \Pi_m}{\partial \rho_{i,j}}$ and $\frac{\partial \Pi_e}{\partial \rho_{i,j}}$ are derived by chain rules, respectively

$$\frac{\partial \Pi_m}{\partial \rho_{i,j}} = \frac{\partial \Pi_m}{\partial \bar{\bar{\rho}}_{i,j}} \cdot \frac{\partial \bar{\bar{\rho}}_{i,j}}{\partial \bar{\rho}_{i,j}} \cdot \frac{\partial \bar{\rho}_{i,j}}{\partial \rho_{i,j}} \tag{C7}$$

$$\frac{\partial \Pi_e}{\partial \rho_{i,j}} = \frac{\partial \Pi_e}{\partial \bar{\bar{\rho}}_{i,j}} \cdot \frac{\partial \bar{\bar{\rho}}_{i,j}}{\partial \bar{\rho}_{i,j}} \cdot \frac{\partial \bar{\rho}_{i,j}}{\partial \rho_{i,j}} \tag{C8}$$

Furthermore, $\frac{\partial \Pi_m}{\partial \bar{\bar{\rho}}_{i,j}}$ and $\frac{\partial \Pi_e}{\partial \bar{\bar{\rho}}_{i,j}}$ is explicit calculated by introducing an adjoint vector $\boldsymbol{\lambda}^c$ and $\boldsymbol{\lambda}^e$, respectively. The corresponding Lagrangian equations are constructed as:

$$L_{\Pi_m} = \Pi_m - \boldsymbol{\lambda}_1^c (\mathbf{K}_{tot} \mathbf{U}_{tot} - \mathbf{F}_{tot}) - \boldsymbol{\lambda}_2^c (\overline{\mathbf{K}_{tot} \mathbf{U}_{tot}} - \overline{\mathbf{F}_{tot}}) \tag{C9}$$

$$L_{\Pi_e} = \Pi_e - \boldsymbol{\lambda}_1^e (\mathbf{K}_{tot} \mathbf{U}_{tot} - \mathbf{F}_{tot}) - \boldsymbol{\lambda}_2^e (\overline{\mathbf{K}_{tot} \mathbf{U}_{tot}} - \overline{\mathbf{F}_{tot}}) \tag{C10}$$

where the discrete system of coupling equilibrium equation $\mathbf{K}_{tot} \mathbf{U}_{tot} = \mathbf{F}_{tot}$ is defined in (**??**), while $\overline{\mathbf{K}_{tot} \mathbf{U}_{tot}} = \overline{\mathbf{F}_{tot}}$ is the corresponding conjugate counterpart. Both equilibrium equations hold for arbitrary $\boldsymbol{\lambda}^c$ and $\boldsymbol{\lambda}^e$. The sensitivities of the Lagrangian equations with respect to $\bar{\bar{\rho}}_{i,j}$ are written

as

$$\frac{\partial L_{\Pi_m}}{\partial \bar{\bar{\rho}}_{i,j}} = \frac{\partial \Pi_m}{\partial \bar{\bar{\rho}}_{i,j}} + \frac{\partial \Pi_m}{\partial \mathbf{U}_{tot}} \cdot \frac{\partial \mathbf{U}_{tot}}{\partial \bar{\bar{\rho}}_{i,j}} + \frac{\partial \Pi_m}{\partial \overline{\mathbf{U}_{tot}}} \cdot \frac{\partial \overline{\mathbf{U}_{tot}}}{\partial \bar{\bar{\rho}}_{i,j}} - \boldsymbol{\lambda}_1^c \frac{\partial (\mathbf{K}_{tot}\mathbf{U}_{tot} - \mathbf{F}_{tot})}{\partial \bar{\bar{\rho}}_{i,j}} - \boldsymbol{\lambda}_2^c \frac{\partial (\overline{\mathbf{K}_{tot}\mathbf{U}_{tot}} - \overline{\mathbf{F}_{tot}})}{\partial \bar{\bar{\rho}}_{i,j}} \tag{C11}$$

$$\frac{\partial L_{\Pi_e}}{\partial \bar{\bar{\rho}}_{i,j}} = \frac{\partial \Pi_e}{\partial \bar{\bar{\rho}}_{i,j}} + \frac{\partial \Pi_e}{\partial \mathbf{U}_{tot}} \cdot \frac{\partial \mathbf{U}_{tot}}{\partial \bar{\bar{\rho}}_{i,j}} + \frac{\partial \Pi_e}{\partial \overline{\mathbf{U}_{tot}}} \cdot \frac{\partial \overline{\mathbf{U}_{tot}}}{\partial \bar{\bar{\rho}}_{i,j}} - \boldsymbol{\lambda}_1^e \frac{\partial (\mathbf{K}_{tot}\mathbf{U}_{tot} - \mathbf{F}_{tot})}{\partial \bar{\bar{\rho}}_{i,j}} - \boldsymbol{\lambda}_2^e \frac{\partial (\overline{\mathbf{K}_{tot}\mathbf{U}_{tot}} - \overline{\mathbf{F}_{tot}})}{\partial \bar{\bar{\rho}}_{i,j}} \tag{C12}$$

We finally obtain the sensitivities of mechanical and electrical energy w.r.t $\bar{\bar{\rho}}_{i,j}$,

$$\frac{d\Pi_m}{d\bar{\bar{\rho}}_{i,j}} = \frac{1}{2}\overline{\mathbf{U}}^T \frac{\partial \mathbf{K}_{uu}}{\partial \bar{\bar{\rho}}}\mathbf{U} - Re\left\{ (\boldsymbol{\lambda}_1^c)^T \frac{\partial \overline{\mathbf{K}_{tot}}}{\partial \bar{\bar{\rho}}} \overline{\mathbf{U}_{tot}} + (\boldsymbol{\lambda}_2^c)^T \frac{\partial \mathbf{K}_{tot}}{\partial \bar{\bar{\rho}}} \mathbf{U}_{tot} \right\} \tag{C13}$$

$$\frac{d\Pi_e}{d\bar{\bar{\rho}}_{i,j}} = \frac{1}{2}\overline{\mathbf{\Phi}}^T \frac{\partial \mathbf{K}_{\phi\phi}}{\partial \bar{\bar{\rho}}}\mathbf{\Phi} - Re\left\{ (\boldsymbol{\lambda}_1^e)^T \frac{\partial \overline{\mathbf{K}_{tot}}}{\partial \bar{\bar{\rho}}} \overline{\mathbf{U}_{tot}} + (\boldsymbol{\lambda}_2^e)^T \frac{\partial \mathbf{K}_{tot}}{\partial \bar{\bar{\rho}}} \mathbf{U}_{tot} \right\} \tag{C14}$$

where $Re\{\cdot\}$ mean the real part of the complex. The adjoint vectors are calculated by the following adjoint equations

$$\overline{\mathbf{K}_{tot}}\boldsymbol{\lambda}_1^c = \frac{\partial \Pi_m}{\partial \overline{\mathbf{U}_{tot}}} \tag{C15}$$

$$\mathbf{K}_{tot}\boldsymbol{\lambda}_2^c = \frac{\partial \Pi_m}{\partial \mathbf{U}_{tot}} \tag{C16}$$

$$\overline{\mathbf{K}_{tot}}\boldsymbol{\lambda}_1^e = \frac{\partial \Pi_e}{\partial \overline{\mathbf{U}_{tot}}} \tag{C17}$$

$$\mathbf{K}_{tot}\boldsymbol{\lambda}_2^e = \frac{\partial \Pi_e}{\partial \mathbf{U}_{tot}} \tag{C18}$$

To solve the adjoint equations, we can use the same mechanical and electric boundary condition as the problem (**??**). The derivatives of material density distribution field $\bar{\bar{\rho}}$ with respect to nodal density field ρ presented in (**??**)-(**??**) can be obtained as

$$\frac{\partial \bar{\bar{\rho}}_{i,j}}{\partial \bar{\rho}_{i,j}} = R_{i,j}^{p,q}(\bar{\xi}, \bar{\eta}) \tag{C19}$$

$$\frac{\partial \bar{\rho}_{i,j}}{\partial \rho_{i,j}} = \frac{w(r_{\bar{i},\bar{j}})}{\sum_{\hat{i}=1}^{n_s}\sum_{\hat{j}=1}^{m_s} w(r_{\hat{i},\hat{j}})} \tag{C20}$$

Substituting (**??**)-(**??**)-(**??**)-(**??**) into (**??**) and (**??**), finally into (**??**), the explicit sensitivity of objection function with respect to nodal density variable ρ can therefore be obtained.

REFERENCES

Q. Deng, M. Kammoun, A. Erturk, and P. Sharma, "Nanoscale flexoelectric energy harvesting," International Journal of Solids and Structures **51**, 3218–3225 (2014).

K. T. V.S. Mashkevich, "Electrical, optical and elastic properties of diamond type crystals," Soviet Physics JETP **5** (1957).

P. Harris, "Mechanism for the shock polarization of dielectrics," Journal of Applied Physics **36**, 739–741 (1965).

S. Kogan, "Piezoelectric effect during inhomogeneous deformation and acoustic scattering of carriers in crystals," Soviet Physics-Solid State **5**, 197 – 224 (1964).

R. Maranganti, N. Sharma, and P. Sharma, "Electromechanical coupling in nonpiezoelectric materials due to nanoscale nonlocal size effects: Green's function solutions and embedded inclusions," Physical Review B **74**, 014110 (2006).

N. Sharma, R. Maranganti, and P. Sharma, "On the possibility of piezoelectric nanocomposites without using piezoelectric materials," Journal of the Mechanics and Physics of Solids **55**, 2328–2350 (2007).

W. Zhu, J. Fu, N. Li, and L. Cross, "Piezoelectric composite based on the enhanced flexoelectric effects," Applied physics letters **89**, 192904 (2006).

S. Shen and S. Hu, "A theory of flexoelectricity with surface effect for elastic dielectrics," Journal of the Mechanics and Physics of Solids **58**, 665–677 (2010).

A. Abdollahi, C. Peco, D. Millán, M. Arroyo, and I. Arias, "Computational evaluation of the flexoelectric effect in dielectric solids," Journal of Applied Physics **116**, 093502 (2014), https://doi.org/10.1063/1.4893974.

A. Abdollahi, D. Millán, C. Peco, M. Arroyo, and I. Arias, "Revisiting pyramid compression to quantify flexoelectricity: A three-dimensional simulation study," Phys. Rev. B **91**, 104103 (2015).

J. Yvonnet and L. Liu, "A numerical framework for modeling flexoelectricity and maxwell stress in soft dielectrics at finite strains," Computer Methods in Applied Mechanics and Engineering **313**, 450 – 482 (2017).

S. Mao, P. Purohit, and N. Aravas, "Mixed finite-element formulations in piezoelectricity and flexoelectricity," Proceedings of the Royal Society A: Mathematical, Physical and Engineering Sciences **472**, 20150879 (2016).

F. Deng, Q. Deng, W. Yu, and S. Shen, "Mixed finite elements for flexoelectric solids," Journal of Applied Mechanics **84** (2017).

T. R. H. Ghasemi, H.S. Park, "A level-set based iga formulation for topology optimization of flexoelectric materials," Computer Methods in Applied Mechanics and Engineering **313**, 239 – 258 (2017).

T. Thai, T. Rabczuk, and X. Zhuang, "A large deformation isogeometric approach for flexoelectricity and soft materials," Computer Methods in Applied Mechanics and Engineering **341**, 718–739 (2018).

B. Nguyen, X. Zhuang, and T. Rabczuk, "Numerical model for the characterization of maxwell-wagner relaxation in piezoelectric and flexoelectric composite material," Computers & Structures **208**, 75–91 (2018).

D. Codony, O. Marco, S. Fernández-Méndez, and I. Arias, "An immersed boundary hierarchical b-spline method for flexoelectricity," Computer Methods in Applied Mechanics and Engineering **354**, 750–782 (2019).

P. V. Yudin and A. K. Tagantsev, "Fundamentals of flexoelectricity in solids," Nanotechnology **24** (2013), 10.1088/0957-4484/24/43/432001.

P. Zubko, G. Catalan, and A. Tagantsev, "Flexoelectric effect in solids," Annual Review of Materials Research **43**, 387–421 (2013).

B. Wang, Y. Gu, S. Zhang, and L.-Q. Chen, "Flexoelectricity in solids: Progress, challenges, and perspectives," Progress in Materials Science **106**, 100570 (2019).

X. Zhuang, B. H. Nguyen, S. S. Nanthakumar, T. Q. Tran, N. Alajlan, and T. Rabczuk, "Computational modeling of flexoelectricity—a review," Energies **13** (2020), 10.3390/en13061326.

J. Fousek, L. Cross, and D. Litvin, "Possible piezoelectric composites based on the flexoelectric effect," Materials Letters **39**, 287–291 (1999).

A. H. Rahmati, S. Yang, S. Bauer, and P. Sharma, "Nonlinear bending deformation of soft electrets and prospects for engineering flexoelectricity and transverse (d 31) piezoelectricity," Soft matter **15**, 127–148 (2019).

J. Yvonnet, X. Chen, and P. Sharma, "Apparent flexoelectricity due to heterogeneous piezoelectricity," Journal of Applied Mechanics **87**, 111003 (2020).

M. P. Bendsøe and N. Kikuchi, "Generating optimal topologies in structural design using a homogenization method," Computer Methods in Applied Mechanics and Engineering **71**, 197 – 224 (1988).

M. P. Bendsøe, "Optimal shape design as a material distribution problem," Structural Optimization **1**, 193–202 (1989).

G. I. Rozvany, M. Zhou, and T. Birker, "Generalized shape optimization without homogenization," Structural optimization **4**, 250–252 (1992).

M. Y. Wang, X. Wang, and D. Guo, "A level set method for structural topology optimization," Computer Methods in Applied Mechanics and Engineering **192**, 227 – 246 (2003).

Y. Xie and G. Steven, "A simple evolutionary procedure for structural optimization," Computers and Structures **49**, 885 – 896 (1993).

R. Balamurugan, C. Ramakrishnan, and N. Singh, "Performance evaluation of a two stage adaptive genetic algorithm (tsaga) in structural topology optimization," Applied Soft Computing **8**, 1607–1624 (2008), soft Computing for Dynamic Data Mining.

G.-C. Luh, C.-Y. Lin, and Y.-S. Lin, "A binary particle swarm optimization for continuum structural topology optimization," Applied Soft Computing **11**, 2833–2844 (2011), the Impact of Soft Computing for the Progress of Artificial Intelligence.

X. yuan YANG and D. WU, "Atomic simulations for surface-initiated melting of nb(111)," Transactions of Nonferrous Metals Society of China **19**, 210–214 (2009).

R. Rao, "Jaya: A simple and new optimization algorithm for solving constrained and unconstrained optimization problems," International Journal of Industrial Engineering Computations **7**, 19–34 (2016).

T. Sang-To, H. Le-Minh, M. Abdel Wahab, and C.-L. Thanh, "A new metaheuristic algorithm: Shrimp and goby association search algorithm and its application for damage identification in large-scale and complex structures," Advances in Engineering Software **176**, 103363 (2023).

T. Nghia-Nguyen, M. Kikumoto, H. Nguyen-Xuan, S. Khatir, M. Abdel Wahab, and T. Cuong-Le, "Optimization of artificial neutral networks architecture for predicting compression parameters using piezocone penetration test," Expert Systems with Applications **223**, 119832 (2023).

Z. Zhang, Y. Li, W. Zhou, X. Chen, W. Yao, and Y. Zhao, "Tonr: An exploration for a novel way combining neural network with topology optimization," Computer Methods in Applied Mechanics and Engineering **386**, 114083 (2021).

V.-T. Tran, T.-K. Nguyen, H. Nguyen-Xuan, and M. Abdel Wahab, "Vibration and buckling optimization of functionally graded porous microplates using bcmo-ann algorithm," Thin-Walled Structures **182**, 110267 (2023).

X. Chen, J. Yvonnet, S. Yao, and H. Park, "Topology optimization of flexoelectric composites

using computational homogenization," Computer Methods in Applied Mechanics and Engineering **381**, 113819 (2021).

X. Chen, J. Yvonnet, H. Park, and S. Yao, "Enhanced converse flexoelectricity in piezoelectric composites by coupling topology optimization with homogenization," Journal of Applied Physics **129**, 245104 (2021), https://doi.org/10.1063/5.0051062.

S. Nanthakumar, X. Zhuang, H. Park, and T. Rabczuk, "Topology optimization of flexoelectric structures," Journal of the Mechanics and Physics of Solids **105**, 217 – 234 (2017).

J. López, N. Valizadeh, and T. Rabczuk, "An isogeometric phase–field based shape and topology optimization for flexoelectric structures," Computer Methods in Applied Mechanics and Engineering **391**, 114564 (2022).

W. Zhang, X. Yan, Y. Meng, C. Zhang, S.-K. Youn, and X. Guo, "Flexoelectric nanostructure design using explicit topology optimization," Computer Methods in Applied Mechanics and Engineering **394**, 114943 (2022).

E. C. N. Silva and N. Kikuchi, "Design of piezoelectric transducers using topology optimization," Smart Materials and Structures **8**, 350 (1999).

C. J. Rupp, A. Evgrafov, K. Maute, and M. L. Dunn, "Design of piezoelectric energy harvesting systems: a topology optimization approach based on multilayer plates and shells," Journal of Intelligent Material Systems and Structures **20**, 1923–1939 (2009).

J. Y. Noh and G. H. Yoon, "Topology optimization of piezoelectric energy harvesting devices considering static and harmonic dynamic loads," Advances in Engineering Software **53**, 45–60 (2012).

E. Nelli Silva, J. Ono Fonseca, F. M. de Espinosa, A. Crumm, G. Brady, J. Halloran, and N. Kikuchi, "Design of piezocomposite materials and piezoelectric transducers using topology optimization—part i," Archives of Computational Methods in Engineering **6**, 117–182 (1999).

E. N. Silva, S. Nishiwaki, and N. Kikuchi, "Design of piezocomposite materials and piezoelectric transducers using topology optimization—part ii," Archives of Computational Methods in Engineering **6**, 191–215 (1999).

T. Hughes, J. Cottrell, and Y. Bazilevs, "Isogeometric analysis: Cad, finite elements, nurbs, exact geometry and mesh refinement," Computer Methods in Applied Mechanics and Engineering **194**, 4135–4195 (2005).

J. A. Cottrell, T. J. Hughes, and Y. Bazilevs, *Isogeometric analysis: toward integration of CAD and FEA* (John Wiley & Sons, 2009).

V. P. Nguyen and S. Bordas, "Extended isogeometric analysis for strong and weak discontinuities," Isogeometric methods for numerical simulation , 21–120 (2015).

T. Cuong-Le, K. D. Nguyen, M. Hoang-Le, T. Sang-To, P. Phan-Vu, and M. A. Wahab, "Nonlocal strain gradient iga numerical solution for static bending, free vibration and buckling of sigmoid fg sandwich nanoplate," Physica B: Condensed Matter **631**, 413726 (2022).

K. D. Nguyen, C.-L. Thanh, F. Vogel, H. Nguyen-Xuan, and M. Abdel-Wahab, "Crack propagation in quasi-brittle materials by fourth-order phase-field cohesive zone model," Theoretical and Applied Fracture Mechanics **118**, 103236 (2022).

X. Chen, S. Yao, and J. Yvonnet, "Dynamic analysis of flexoelectric systems in the frequency domain with isogeometric analysis," Computational Mechanics **71**, 353–366 (2023).

H. Askes and E. Aifantis, "Gradient elasticity in statics and dynamics: An overview of formulations, length scale identification procedures, finite element implementations and new results," International Journal of Solids and Structures **48**, 1962–1990 (2011).

D. Carl, *A practical guide to splines*, Vol. 27 (springer-verlag New York, 1978).

J. Gao, L. Gao, Z. Luo, and P. Li, "Isogeometric topology optimization for continuum structures using density distribution function," International Journal for Numerical Methods in Engineering **119**, 991–1017 (2019), https://onlinelibrary.wiley.com/doi/pdf/10.1002/nme.6081.

J. Gao, L. Wang, Z. Luo, and L. Gao, "Igatop: an implementation of topology optimization for structures using iga in matlab," Structural and Multidisciplinary Optimization **64**, 1669–1700 (2021).

K. Svanberg, "A class of globally convergent optimization methods based on conservative convex separable approximations," SIAM Journal on Optimization **12**, 555–573 (2002).

P. Zubko, G. Catalan, A. Buckley, P. R. L. Welche, and J. F. Scott, "Strain-gradient-induced polarization in srtio$_3$ single crystals," Phys. Rev. Lett. **99**, 167601 (2007).

E. R. Cholleti, "A review on 3d printing of piezoelectric materials," in *IOP conference series: materials science and engineering*, Vol. 455 (IOP Publishing, 2018) p. 012046.

H. Askes and E. C. Aifantis, "Gradient elasticity and flexural wave dispersion in carbon nanotubes," Phys. Rev. B **80**, 195412 (2009).

L. Wang and H. Hu, "Flexural wave propagation in single-walled carbon nanotubes," Phys. Rev. B **71**, 195412 (2005).